THE ORIGIN OF THE KAHNUJ OPHIOLITIC COMPLEX, SE OF IRAN: CONSTRAINTS FROM WHOLE ROCK AND MINERAL CHEMISTRY OF THE BANDE-ZEYARAT GABBROIC COMPLEX

Mohsen Arvin*, Abbed Babaei, Gholamreza Ghadami*, Sara Dargahi*** and **Alireza Shaker Ardekani***

** Dept. of Geology, College of Sciences, Shahid Bahonar University of Kerman, P.O.Box 133-76135, Kerman, Iran (Corresponding author, e-mail: arvin@mail.uk.ac.ir).*

*** Dept. of Biological, Geological and Environmental Sciences, Cleveland State University, Cleveland, OH 44115, USA.*

Keywords: *Ophiolite, gabbro, mineral chemistry, Late Jurassic-Early Cretaceous. Kahnuj, Iran.*

ABSTRACT

The Upper Jurassic-Lower Cretaceous Kahnuj ophiolite complex, a part of Jazmurian ophiolitic belt, is situated in the southeastern part of Iran and represents a remnant of the Mesozoic Neotethyan Ocean. The oceanic lithospheric section of the Kahnuj ophiolite comprises from bottom to top: a plutonic unit (Bande-Zeyarat Complex); a diabase sheeted dyke unit; and a volcanic unit (Dare-Anar Complex). Although it is extensively faulted and fractured, the internal relationships have been preserved. The Bande-Zeyarat gabbroic complex consists of layered gabbroic cumulates and isotropic gabbros. The cumulate gabbro shows adcumulate, mesocumulate and orthocumulate textures and is represented exclusively by olivine gabbro, gabbro, melagabbro, leucogabbro, anorthosite, with minor troctolite, gabbronorite, pegmatoid and tectonic rafts of dunite. The cumulate gabbro is characterized by well-developed magmatic layering, defined by variation in mode /or size of plagioclase and mafic minerals, and by a tectonic foliation which is marked by preferred flattening of all mineral phases. These two structures for most parts are sub-parallel to each other. Rhythmic layering is also present. The isotropic gabbro consists of hypidiomorphic granular uralitized pyroxene gabbro and hornblende gabbro with minor ilmenite-rich gabbro, olivine gabbro, diorite and trondhjemite. They are the most fractionated part of the gabbros, plagioclase is more albite rich, clinopyroxene and olivine are more iron rich. The layered gabbro shows strong positive Eu anomalies, attributable to high modal abundances of plagioclase, whereas the isotropic gabbro with hornblende predominant over plagioclase does not have any Eu anomalies. The isotropic gabbros are crystallized from influxes of slightly different less magnesiferous parental melts. They are related to the cumulate gabbro by crystal fractionation and represent late differentiation products which formed as the rate of the magma influx slowed and finally ceased. Mineral assemblages, mineral chemistry (i.e., $Fo_{67.8\text{-}78.54}$, low Mg# < 84.16 and high Si relative to tetrahedral Al in clinopyroxenes), crystallization order (olivine-plagioclase-clinopyroxene) and whole rock chemistry suggest that the Bande-Zeyarat gabbroic complex has been produced by low to moderate pressure crystal fractionation from a tholeiitic basaltic magma similar to MORB. These data indicate that the Kahnuj ophiolite complex may represent an oceanic basin developed in the Mesozoic between the Lut block of Central Iran and the Bajgan-Dur-Kan microcontinents.

INTRODUCTION

Ophiolite in its modern definition is “an oceanic magmatic complex that consists (from bottom to top) of ultramafic rocks, with variable amount of commonly serpentinized harzburgite, lherzolite and dunite, overlain by layered/non-layered gabbroic rocks which form beneath extrusive rocks, such as basalt, with or without a sheeted dyke complex, and finally, a package of pelagic deep-sea sediments” (Robertson, 2002).

As remnants of obducted oceanic crust, ophiolites mark the presence of former suture zones and play an important role in plate tectonic reconstructions (Coleman, 1977; Moores, 1982). The diversity of Mesozoic ophiolites and associated oceanic magmatic units of the Middle East has been the subject for many workers in recent years. These ophiolites are exposed in elongated belts along the northern margin of the Afro-Arabian Plate (e.g. Tauride of Turkey, Neyriz of Iran, Semail of Oman) and represent variably disrupted fragments of the Neotethyan Ocean that developed between Eurasia and Gondawana land in the Triassic (Berberian and King, 1981; Sengor, 1987; 1990; Moores et al., 2000). In contrast to the settings of Modern oceanic lithosphere, the various Middle East ophiolites have different origins and formed in a variety of tectonic settings (e.g. Oman and Tauride ophiolites have supra-subduction zone components, Masireh Island of Oman has MORB affinity).

The Mesozoic suture zones in Iran (Fig. 1a) are marked by numerous tectonically deformed ophiolite complexes. Some studies suggest a single ocean model (Ricou, 1971) for the origin of these suture zones and ophiolites, while others (Berberian and King, 1981; Knipper et al., 1986) suggest that the Mesozoic ophiolite units formed in different ocean basins with different tectonic settings. The latter view has the merit to explain the abundant volcanic rocks which represent different tectonic settings.

In general, the Iranian Neotethyan ophiolites are found in three distinct tectonic trends (Fig. 1a): a southern NW-SE trending belt [Peri-Arabic belt of Ricou (1971) or Southern Neotethyan Ocean of Sengor (1990)], the N-S and E-W trending, Central Iranian belt which represents the remnants of the Nain-Baft and Sabzevaran-Sistan oceans (McCall and Kidd, 1981; Tirrul et al., 1983; McCall, 1997), and the 150 km wide, NW-SE and E-W trending, Jazmurian belt which marks the remnants of the Lower Cretaceous Makran ocean basin or Inner Makran spreading zone (Inner Makran Suture of McCall and Kidd, 1981) between the Lut block and Bajgan-Dur-Kan microcontinents (a southern continuation of the Sanandaj-Sirjan microcontinent). The well-preserved Kahnuj ophiolite belongs to this relatively large ophiolite belt.

The general regional geology of the Iranian Makran mountain range (including the Kahnuj ophiolitic belt) appears in a map by McCall (1985) who worked for Paragon-Contech (an Australian Company) on contract for the Geological and Mineralogical Survey of Iran. A detailed geochemical, petrological, geochronological, and tectonic interpretation of the Kahnuj ophiolitic complex has recently been the subject of some studies (Hassanipak et al., 1996; McCall, 1997; Arvin et al., 2001; Kananian et al., 2001; Ghazi

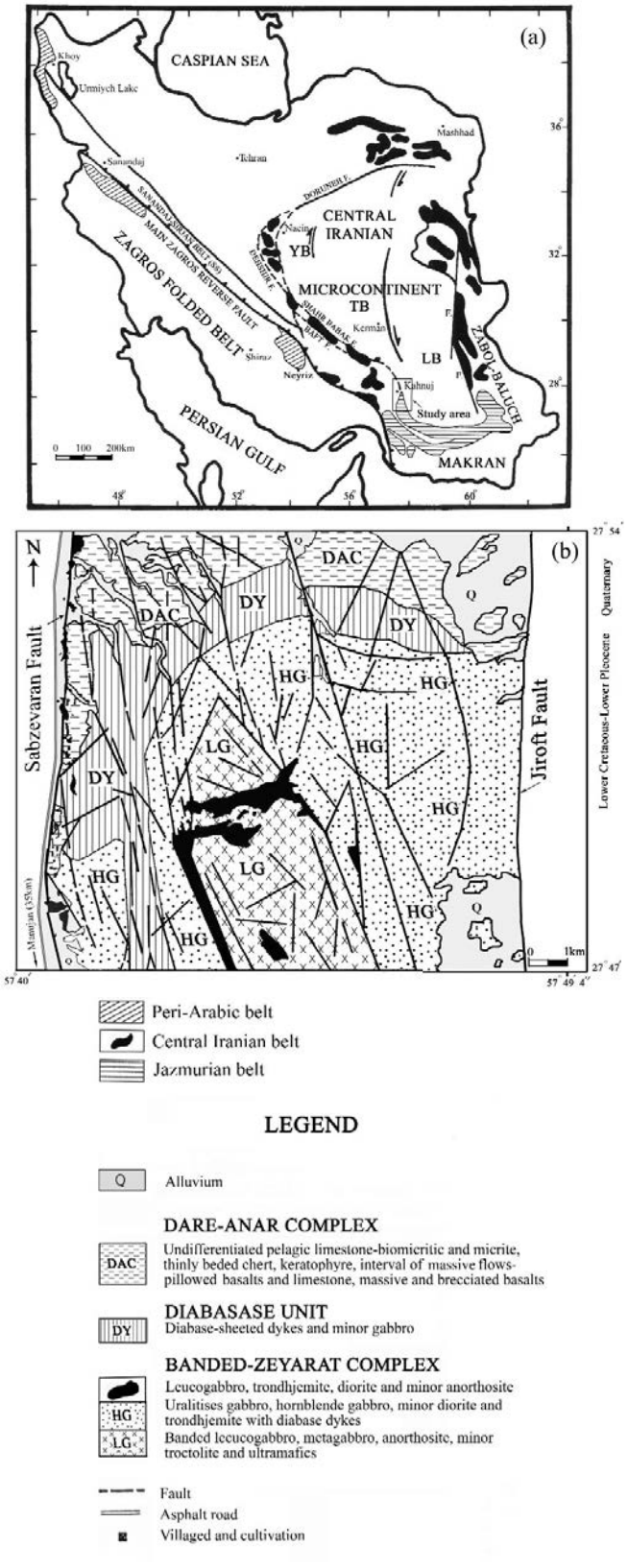

Fig. 1 - (a) Distribution of Iranian Mesozoic ophiolites. (b) Geological map of the Kahnuj ophiolite complex, southeast of Kahnuj, Kerman (modified from Arvin et al., 2001).

et al., 2004). The purpose of this paper is to present new microprobe data and major and trace element analyses to shed some light on the magmatic and petrogenetic processes of the Bande-Zeyarat gabbroic section and to investigate its tectonic environment of formation.

REGIONAL SETTING

The Kahnuj ophiolite complex is bounded to the east and west by two major north-south trending fault systems: the Sabzevaran and Jiroft faults (Fig. 1b). Although the complex is extensively faulted and fractured, its structure is well preserved in a few outcrops. The field relationships and fossil content of ophiolite related sediments (i.e. in the pelagic limestones interbedded with the pillow lavas and massive lava flows) indicate that Kahnuj ophiolite is Early Cretaceous to Early Paleocene in age. The K-Ar age dating by McCall (1985), Hassanipak et al. (1996) and Kananian et al. (2001) also suggest an Early Cretaceous to Early Paleocene age, whereas $^{40}Ar/^{39}Ar$ age dating by Ghazi et al. (2004) suggests a Late Jurassic-Early Cretaceous age for these rocks.

The Kahnuj ophiolitic complex covers an area of ~800 km^2 (Fig. 1b) and consists of the Bande-Zeyarat plutonic complex at the bottom, the diabase sheeted dyke complex in the middle, and the Dare-Anar volcanic complex on top (McCall, 1985).

The Bande-Zeyarat plutonic complex

The plutonic rocks of the Bande-Zeyarat Complex resemble a classic ophiolite sequence, with cumulate layered gabbro in the lower section and isotropic gabbro on top. The contact between cumulate and isotropic gabbros is transitional; sheared and mylonitized zones of layered and isotropic gabbros are exposed in many places along the contact near the bottom of the isotropic gabbro.

The layered or low-level gabbro which comprises most of the Bande-Zeyarat complex includes banded cumulate gabbro, olivine gabbro, gabbro, melagabbro, leucogabbro, anorthosite, and minor troctolite, gabbronorite, pegmatoid and tectonic rafts of dunite. A steep east-dipping banding and rhythmic layering is common in the low-level gabbro. The rhythmic banding and gradual modal variations at the layer scale are scarce and the layers are lens-shaped (McCall, 1985). The ubiquitous cumulus layering has a variable thickness from few centimeters to meters, and is marked by well-developed cumulus textures. The magmatic layering is defined either by the relative abundance and distribution or the size of the three primary cumulus phases (olivine, plagioclase and clinopyroxene). A distinct tectonic foliation defined by preferred orientation of all mineral phases is recorded in these rocks. Indeed, some features are indicative of large strains at magmatic temperatures: for example, boudinage and tight folds. McCall (1985) believes that magmatic layering and tectonic foliation are generally parallel (oriented north-south). Locally, lattice preferred orientations in olivine and plagioclase are oblique to banding, indicating a component of simple shear. However, most deformation could have been pure shear; that is mechanical flattening and diffusion creep during compaction as it has been also reported from Oman (Kelemen et al., 1997).

The isotropic or high-level gabbro is mildly weathered and is composed of non-cumulate gabbro with xenomorphic texture. This unit consists of coarse grained uralitized pyroxene gabbro, hornblende gabbro with often pegmatoid texture, and minor ilmenite-bearing gabbro, olivine gabbro, diorite and trondhjemite. The ilmenite-bearing gabbro, which is the source of the ilmentite placer deposits in this area (Sabzehi et al., 1993), occurs in the western margin of the complex. Xenoliths of cumulate gabbros are abundant in the isotropic gabbro. The high-level gabbro grades texturally into sheeted dykes, where their original contact is preserved.

Diabase sheeted dyke unit

The sheeted dyke unit comprises a set of north-south trending subvertical doleritic dykes rooted in the isotopic gabbro. The dykes make up to 98% of the rock mass. The sheeted dyke complex shows typical asymmetrical chilled margins and their width varies from 0.5 to 5 m. There are also isolated dykes intruded in the isotropic gabbros with symmetrical chilled margins. Adjacent to the diabase unit, hornblende gabbro, trondhjemite and plagioclase-phyric microdiorite are intimately mixed up in a complex agmatite with a variety of marginal relationships.

Leucocratic bodies of trondhjemitic plagiogranites, granite, tens or hundreds of meters across with occasional gradation into diorites, intrude the gabbro and diabase sheeted dykes as diffuse segregations or discontinuous sheeted-like bodies.

Dare-Anar complex

This extrusive unit consists mainly of basaltic and basaltic-andesite pillow lavas interbedded with few massive lava flows and pillow breccias. The massive flows show gentle flexuring. Individual flows can be distinguished by their brecciated margins and the interlayered thinly bedded Aptian-Cenomanian pelagic limestone (Arvin et al., 2001). The limestone marks a depositional contact with basaltic rocks and becomes more abundant towards the top of the Dare-Anar complex.

PETROGRAPHIC FEATURES OF GABBROIC ROCKS

The layered gabbro is characterized by adcumulate, mesocumulate and orthocumulate textures. The average grain size in this rock varies from fine (< 1mm) to medium (1-4 mm) and changes to coarse grains (4-30 mm) in irregular veins and patches. In pegmatitic veins, the average crystal size ranges between 3 and 15 cm.

Layering is common in most of the cumulus gabbro. The layer is defined by bands of mafic and felsic minerals; these bands are mostly at microscopic scale, although macroscopic scale banding is also seen in a few outcrops. The individual layers in cumulate gabbro cannot be traced more than a few meters. This is due either to the layers pinch outs or to transition from one rock type to another along strike.

The cumulate gabbro consists mainly of olivine, plagioclase, clinopyroxene as cumulus phases (in this order of crystallization), and < 5% orthopyroxene and hornblende (uralite). The lack of additional cumulus phases (orthopyroxene, hornblende, and magnetite) within the cumulate gabbro shows that the bulk of magma did not undergo strong fractionation during cumulus crystallization. Olivine cumulus crystals have variable shapes, from subidiomorphic to rounded. The plagioclase minerals are the second most abundant early euhedral-subhedral cumulus phase and variable in size, with ubiquitous albite-carlsbad and polysynthetic twinning, often exhibiting 120^{o} triple junctions. They are included in centimeter-sized poikilitic clinopyroxene crystals. Clinopyroxene, between 0.4 and 2.8 mm in size, is generally present as subhedral-anhedral to poikilitic intercumulate phase, with plagioclase inclusions. Tiny opaque oxides inclusions also formed along the pyroxene cleavages (schillerian texture).

The isotropic gabbro has hypidiomorphic granular to pegmatoid textures. Variable grain size and non-homogeneous content of clinopyroxene, plagioclase, hornblende, Fe-Ti oxides, and scarce olivine, reflect static (non-cumulus) crystallization under variable fO_2 and f H_2O.

Pervasive subsolidus hydrous alteration of the Bande-Zeyarat gabbro implies the replacement of: (1) clinopyroxene and hornblende by pale green fibrous actinolitic amphibole (uralite), (2) olivine by serpentine, and by (3) saussuritization of calcic plagioclase. The pseudomorphic nature of secondary minerals and the lack of an accompanying metamorphic texture suggest that this alteration is hydrothermal in origin, although the intensity of this alteration varies in different samples. Similar features are reported from other ophiolite complexes (e.g., Gass and Smewing, 1973; Hopper and Smith, 1996; Parlak et al., 2002).

ANALYTICAL TECHNIQUES

A total of 25 less altered samples were collected from the cumulate and isotropic gabbros for major and trace element analyses. The analyses were performed at the College of Oceanic and Atmospheric Sciences at Oregon State University. The major and trace elements were analyzed by the Varian inductively coupled plasma-atomic emission spectrometer (ICP-AES). About 0.1g of each powdered sample was mixed with 0.9g lithium borate flux in a carbon crucible and heated in a furnace at 1100ºC for 30 minutes. The fused glass samples were dissolved (using a magnetic stirring device) in 100 ml of 1% HNO_3 solution with Germanium as internal standard. Dissolution of international basalt standards was chosen for calibration. Based on the analyses of international reference materials, the major oxides are estimated to be accurate within 0.1 wt.%.

The rare earth element contents (REE), Hf, Ta, Th and Nb on 10 samples were determined by inductively coupled plasma mass spectrometry (ICP-MS) techniques. The sample powder (0.08 g) was dissolved, using a mixture of HF, HCl, and HNO_3 in special screw-top plastic vials. An internal standard solution containing the Indium element was then added and the spiked sample dissolution were diluted with 1% HNO_3. The internal standard was used for monitoring drift in mass response during mass spectrometric measurements. Dissolution of BCR-1, W2, IB-1a and BIR-1 were chosen as calibration standards for element concentrations of the measured samples (Govindaraju and Mevelle, 1987; Voldet, 1993). The precision and accuracy of the trace-element analyses are estimated to be better than 5%, except for Nb and Ta (better than 9%). Details of the ICP-MS technique can be found in Xie et al. (1993; 1994).

The compositions of three primary minerals of the Bande-Zeyarat gabbro were analyzed using an automated Camebax SX-50 in the Geoscience Department at Oregon State University. An accelerating voltage of 15 KV and beam current of 50 nA were applied with a counting time of 20 seconds. Chemical compositions of the olivine, plagioclase and clinopyroxene in the gabbroic rocks are shown in Fig. 5.

WHOLE ROCK CHEMISTRY

Table 1 shows the concentration of major and trace elements of the cumulate and isotropic gabbros. This study was conducted to investigate the context of the chemical variation in the Bande-Zeyarat sequence.

Table 1 - Representative whole rock analyses of the Bande-Zeyarat gabbro complex.

Sample	CGQ14	CGQ15	CGQ16	CGQ18	CGQ19	CGQ20	CGQ27	CGQ44	CGQ45	CGQ46	CGQ55	CGQ59	CGQ60
Wt%													
SiO_2	48.45	49.46	49.09	50.68	48.59	48.93	48.39	48.96	49.76	49.06	43.78	44.09	44.37
TiO_2	0.24	0.37	0.43	0.32	0.15	0.30	0.23	0.29	0.28	0.60	0.21	0.15	0.17
Al_2O_3	16.82	15.72	15.29	17.91	17.11	17.13	17.39	17.92	17.62	18.08	16.38	12.39	19.27
FeO^*	9.48	9.82	9.56	6.25	8.87	7.65	5.84	8.07	6.22	5.92	8.91	11.31	9.05
MnO	0.15	0.12	0.16	0.10	0.10	0.14	0.10	0.07	0.11	0.14	0.11	0.21	0.10
MgO	11.78	11.46	11.71	9.79	11.40	11.64	10.39	7.37	8.14	7.94	13.38	20.96	10.85
CaO	11.76	10.85	10.69	10.84	9.89	11.55	13.01	12.77	14.67	15.35	10.33	4.30	11.39
Na_2O	1.76	1.58	1.70	2.51	1.72	1.99	1.98	2.32	1.60	1.63	1.88	1.33	1.83
K_2O	0.09	0.05	0.02	0.12	0.03	0.07	b.d.	0.11	0.03	0.17	0.04	0.01	0.03
P_2O_5	0.02	0.01	0.01	0.01	0.01	0.13	0.01	0.01	0.04	0.08	0.01	0.01	0.01
LOI	0.01	0.03	0.31	0.35	1.32	0.38	3.13	2.13	0.57	0.47	3.71	6.23	2.22
Total	100.56	99.47	98.97	98.88	99.19	99.91	100.47	100.02	99.04	99.44	98.74	100.99	99.29
Mg#	55.41	53.85	55.05	61.03	56.24	60.34	64.02	47.73	56.69	57.29	60.03	64.95	54.52
ppm													
Sc	14	29	26	38	7	24	30	25	31	44	24	16	12
V	55	113	104	141	40	82	99	84	103	177	73	47	49
Cr	221	204	659	601	109	497	764	388	602	784	340	347	196
Ni	252	75	144	73	194	251	207	39	425	160	122	951	282
Cu	80	n.d.	n.d.	25	n.d.	64	n.d.	n.d.	n.d.	72	n.d.	155	75
Zn	50	n.d.	n.d.	20	n.d.	47	n.d.	n.d.	n.d.	39	n.d.	61	26
Sr	276	171	193	300	200	258	216	244	161	230	137	95	316
Ba	16	b.d.	b.d.	18	b.d.	20	4	20	10	15	1	6	20
Y	4	4	4	8	3	9	5	n.d.	n.d.	1	8	3	3
Zr	7	12	14	10	8	22	13	12	b.d.	11	19	4	6
Nb	0.64			0.57		0.85				0.76		0.50	0.62
Rb	0.39			0.32		0.14				0.27		0.17	0.33
Hf	0.14			0.35		0.55				0.42		0.11	0.14
Ta	0.09			b.d.		b.d.				0.08		b.d.	b.d.
Th	b.d.			b.d.		b.d.				b.d.		b.d.	b.d.
Lu	0.05			0.09		0.12				b.d.		b.d.	b.d.
U	b.d.			b.d.		0.01				0.85		0.21	0.61
Ce	1.68			2.10		3.80				2.60		0.72	1.63
Pr	0.27			0.41		0.63				0.48		0.15	0.29
Nd	1.27			2.14		3.17				2.57		0.60	1.25
Sm	0.38			0.82		1.01				0.92		0.26	0.39
Eu	0.43			0.63		0.58				0.56		0.19	0.42
Gd	0.52			1.06		1.13				1.32		0.34	0.48
Tb	0.08			0.19		0.20				0.23		0.06	0.07
Dy	0.47			1.26		1.28				1.49		0.37	0.41
Ho	0.12			0.27		0.29				0.34		0.09	0.10
Er	0.29			0.73		0.82				0.85		0.23	0.23
Tm	0.04			0.10		0.13				0.12		0.03	0.03
Yb	0.32			0.67		0.78				0.83		0.27	0.26
La	0.64			0.74		1.45				0.11		0.05	0.04
La_N/Yb_N	1.44			0.79		1.33				0.73		0.55	1.68
Nb/Y	0.15			0.07		0.09				0.07		0.17	0.21

Sample	CGQ61	CGQ62	CGQ64	CGQ72	IGQ7	IGQ8	IGQ10	IGQ12	IGQ13	IGQ51	IGQ78	IGQ84
Wt%												
SiO_2	48.26	47.37	49.11	49.78	49.27	44.16	48.42	49.94	48.70	49.88	49.23	48.80
TiO_2	0.38	0.20	0.19	0.22	1.31	2.71	1.52	1.94	1.25	1.52	1.48	2.71
Al_2O_3	18.81	16.39	17.41	19.08	15.91	16.49	15.68	14.37	17.38	14.92	17.56	17.80
FeO^*	5.07	9.02	7.76	6.42	10.69	11.37	11.43	10.54	9.48	10.71	10.07	9.94
MnO	0.10	0.13	0.10	0.12	0.15	0.16	0.19	0.17	0.17	0.16	0.17	0.19
MgO	9.13	12.63	10.17	8.81	6.35	7.66	8.28	8.45	5.61	9.82	6.88	4.88
CaO	14.12	10.86	12.22	13.90	9.48	14.71	10.54	10.37	14.82	10.69	11.11	11.14
Na_2O	2.99	1.27	1.99	1.83	5.05	2.48	1.97	2.78	2.34	2.56	2.01	2.92
K_2O	0.07	0.03	0.02	0.01	0.44	0.07	0.11	0.08	0.14	0.02	0.08	0.23
P_2O_5	0.01	0.01	0.01	b.d.	0.12	0.57	0.17	0.21	0.16	0.13	0.17	0.51
LOI	0.35	1.21	0.70	0.63	0.12	0.27	1.38	0.12	0.33	0.13	0.28	0.48
Total	99.29	99.12	99.68	100.80	98.89	100.65	99.69	98.97	100.38	100.54	99.04	99.60
Mg#	64.30	58.34	56.72	10.18	37.27	57.85	42.01	44.50	37.18	47.83	40.59	32.93
ppm												
Sc	31	20	27	37	36	23	42	27	26	33	34	42
V	109	72	94	101	251	265	327	223	196	225	261	274
Cr	764	590	369	670	135	92	159	45	252	94	151	19
Ni	79	280	105	165	62	67	73	b.d.	88	21	71	b.d.
Cu	n.d.	n.d.	25	22	44	n.d.	72	n.d.	n.d.	n.d.	n.d.	n.d.
Zn	n.d.	n.d.	21	28	87	n.d.	94	n.d.	n.d.	n.d.	n.d.	n.d.
Sr	204	140	293	219	239	228	228	180	152	178	168	230
Ba	2	b.d.	24	9	107	23	70	176	76	29	30	26
Y	5	3	5	5	39	43	4	35	26	32	52	55
Zr	16	9	4	8	16	57	42	77	24	61	n.d.	106
Nb			0.53	0.59	6.84		4.17					
Rb			0.19	0.25	0.56		0.59					
Hf			0.12	0.22	0.63		2.12					
Ta			0.06	0.06	0.47		0.22					
Th			b.d.	b.d.	0.10		0.06					
U			b.d.	b.d.	0.06		0.48					
La			0.48	0.30	10.60		0.05					
Ce			1.31	1.10	25.50		14.80					
Pr			0.25	0.23	3.62		2.48					
Nd			1.29	1.20	16.46		12.19					
Sm			0.54	0.49	4.71		3.99					
Eu			0.42	0.33	1.74		1.45					
Gd			0.73	0.74	5.24		4.52					
Tb			0.13	0.12	0.96		0.87					
Dy			0.81	0.80	6.06		5.63					
Ho			0.19	0.19	1.32		1.23					
Er			0.47	0.46	3.70		3.46					
Tm			0.07	0.06	0.60		0.55					
Yb			0.45	0.44	3.70		3.30					
Lu			0.06	0.07	0.56		5.06					
La_N/Yb_N			0.76	0.48	2.05		1.10					
Nb/Y			0.11	0.12	0.17		0.11					

Note: total Fe as FeO*, b.d.=below detection limit, n.d.=not determined.. CG=Cumulate gabbro, IG=Isotropic gabbro.

The cumulate gabbro is characterized by low values of TiO_2 (0.15-0.60%), K_2O (0.01-0.17%), P_2O_5 (0.002-0.13%), large-ion lithophile elements (LILE) such as Ba (1.41-24 ppm), other incompatible elements, i.e, Zr (4-22 ppm), Y (3-10 ppm) and REE. In contrast, the concentrations of Al_2O_3 (12.39-19.27%), CaO (4.23-15.35%) and MgO (7.37-13.38%) are relatively high (Table 1).

The isotropic gabbros are characterized by higher TiO_2 (1.25-2.71%), K_2O (0.02-0.44%), P_2O_5 (0.12-0.57%), and rich in compatible trace elements compared to the cumulate gabbro (Table 4). Low Nb/Y in the isotropic (0.11-0.17) and cumulate (0.07-0.21) gabbros reflect a subalkaline (tholeiitic) basalt as the original magma (Winchester and Floyd, 1977). Further evidence of their tholeiitic nature and differentiation trend is also shown on the AFM diagram (Fig. 2).

The cumulate gabbro is depleted in Zr and Y; in contrast the isotropic gabbro has higher Zr and Y contents, probably due to the presence of a significant amount of Zr-rich trapped liquid. The concentration of V in the isotropic gabbro is also higher than in cumulate gabbro. This may be due to the effect of the vanadium-rich ilmenite and magnetite in isotropic gabbro.

The major element chemistry and abundance of compatible trace elements such as Ni and Cr vary with the modal abundance of the cumulus phases. The low concentrations of the incompatible trace elements may be justified by the high proportion of cumulus minerals and the low amount of intercumulus liquid in the magma chamber of the Bande-Zeyarat gabbros. Cumulate gabbros of the same type and geochemistry are also reported from the upper part of the cumulate section in the Pozantı-Karsantı ophiolite in Turkey (Parlak et al., 2000) and from the gabbroic complex in Oman (Kelemen et al., 1997).

Major element compositions of the Bande-Zeyarat gabbros are also plotted in the AFM diagram of Beard (1986). The cumulate gabbro plots in the arc-related mafic cumulate field, whereas the isotropic gabbro plots in the arc related non-cumulate field (Fig. 2). This may imply that both the cumulate and non-cumulate gabbros, having a supra-subduction zone signature, were formed in a back arc basin tectonic setting.

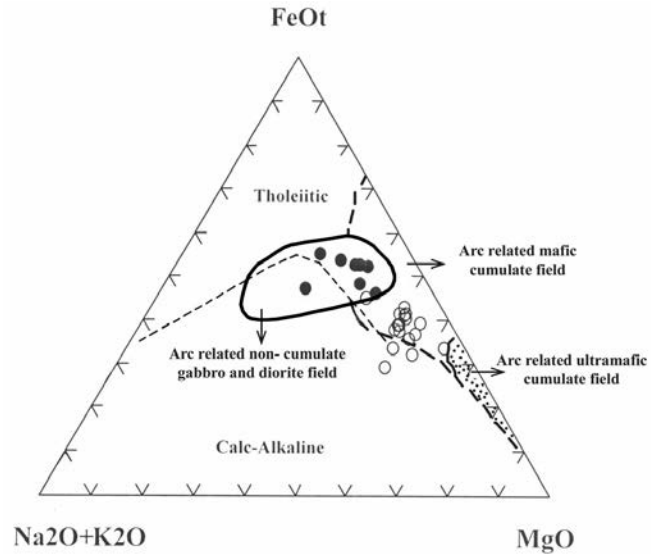

Fig. 2 - AFM compositions of the Bande-Zeyarat gabbro complex. Field of cumulate and non-cumulate rocks is from Beard (1986). Tholeiitic and calc-alkaline boundary from Kuno (1968). ○, Cumulate gabbro; ●, Isotropic gabbro.

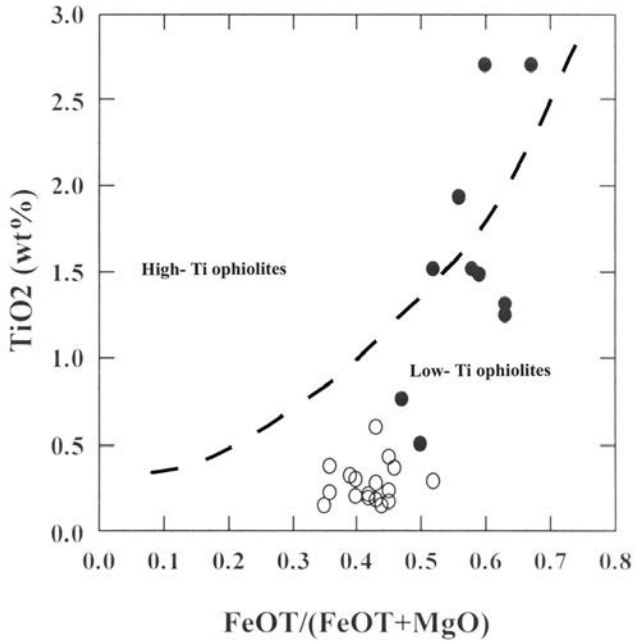

Fig. 3 - Variation of TiO_2 content *vs.* FeOt/(Feot+MgO) of the Bande-Zeyarat gabbro complex (Serri, 1981). See Fig. 2 for key to symbols.

The amount and concentration of TiO_2 is crucial in understanding the original magma and diversity of ophiolites as it is shown in TiO_2 vs. FeOt/(FeOt + MgO) diagrams (see Bébien, 1972; Beccaluva et al., 1979; Serri, 1981; Zhihong and Huafu, 1998). In Fig. 3, low-level gabbro falls within the fields of high and low-Ti ophiolites, whereas high-level gabbro falls within the field of high-Ti ophiolite. However it is clear that with increasing of fractionation index from cumulate towards isotropic gabbros the rocks intended to fall within the high-Ti field, similar to fractionation of oceanic

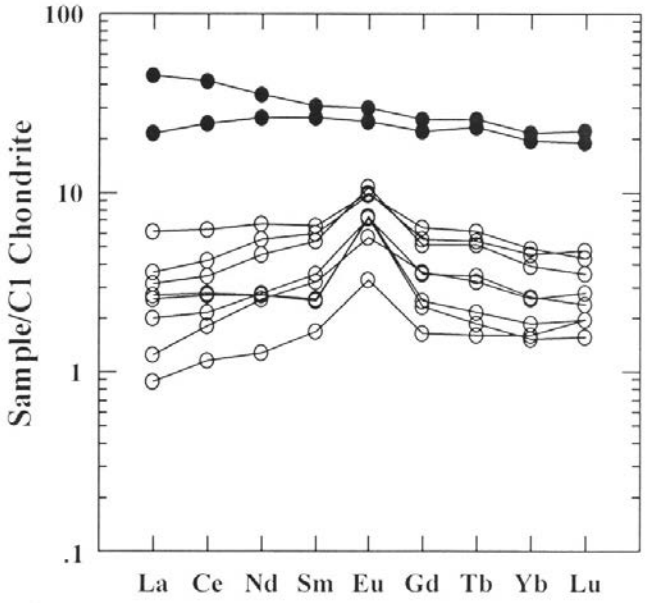

Fig. 4 - REE patterns of the Bande-Zeyarat gabbro complex. See Fig. 2 for key to symbols. Normalizing values are from Sun and McDonough (1989). See Fig. 2 for key to symbols.

gabbros (Serri, 1981). Thus, with regards to parental magmas for low and high-Ti ophiolites, it can be concluded that partial melting processes occurring in the mantle gave rise to the formation of low and high Ti magmas.

The REE concentrations of 8 cumulate gabbros and 2 isotropic gabbros are given in Table 1 and are plotted in Fig. 4. REE patterns clearly distinguish the two units in the Bande-Zeyarat complex. The REE patterns of the layered gabbro are obviously controlled by plagioclase, clinopyroxene and to some extent olivine. The plagioclase prefers LREE over HREE, whereas the reverse hold for clinopyroxene, and also preferentially concentrates Eu^{2+} relative to the other trivalent REE contents (Lipin and McKay, 1989; Barling et al., 1997). The layered cumulus gabbros show strong LREE and lesser HREE depletions producing a convex-upward pattern at ~2-9x chondritic abundance due to high plagioclase content. Generally, REEs are depleted in cumulate gabbros (as normally expected), and depletion of LREE with respect to HREE is in the normal range for MORB liquids (average La_N/Yb_N = 0.97). Moreover, some samples show LREE enrichment with respect to HREE (La_N/Yb_N = 1.33, 1.68) and there is no definite difference with isotropic gabbros (La_N/Yb_N = 1.1-2.05). Strong, positive Eu anomalies [$(Eu/Eu^*)_{avg}$ = 1.58] are present in all of the low-level cumulate gabbros. The same positive anomalies of Eu with respect to other REE in Oman (Pallister and Knight, 1981) indicate that low-level gabbros do not represent liquid composition, they are cumulate rocks precipitated during crystal fractionation of the cooling magma, from which a large residual liquid fraction was later removed. The convex upward shapes of the patterns (LREE depleted) and positive Eu anomalies are consistent with the known distribution coefficient patterns for the dominant minerals in these gabbros (Hassanipak et al., 1996; Ghadami et al., 2003). These patterns are similar to the general REE patterns of cumulus gabbros reported by Pallister and Knight (1981) and Kelemen et al. (1997).

The isotropic gabbros have higher REE contents with an average of about > 20x enriched relative to the chondrite values and La_N/Yb_N = 1.1-2.05 (Fig. 4). However, these patterns have no Eu anomaly due to the removal of plagioclase. Hornblende is predominant over plagioclase in the isotropic gabbros; plagioclase apparently contributes little to the patterns for these gabbros. Pallister and Knight (1981) have reported similar mineralogical behavior in gabbros of the Semail ophiolite in Oman.

MINERAL CHEMISTRY

Olivine. The result of olivine analyses in cumulate and isotropic gabbros are shown in Table 2. In low-level or cumulate gabbro, olivine is the first mineral that has crystallized as a cumulus phase. It is a magnesian-poor olivine with restricted range in composition ($Fo_{71.29-78.54}$) and a NiO content that ranges from 0.06 to 0.19 (Table 2), zoning is not observed. The average compositions of olivine in the Bande-Zeyarat cumulate gabbro (Table 2) are comparable to phenocryst phases in oceanic basalts (e.g. Stakes et al., 1984), near-liquidus olivine compositions in experimental studies of oceanic basalts (e.g., Grove and Bryan, 1983), and olivine components in cumulate gabbroic rocks from other oceanic localities (e.g., Vanko and Batiza, 1982; Hébert et al., 1983; Elthon, 1987). In high-level or isotropic gabbro, olivine is richer in Fe ($Fo_{67.8-69}$) and its NiO content ranges from 0.03 to 0.06 (Table 2), this may contemplating its fractional crystallization from the lower gabbro. Though this conclusion may be reasonable, one cannot exclude that olivine in high level gabbros may have crystallized from less magnesiferous primitive magmas (from influxes of slightly different parental melts) rather than from the residual after cumulate formation.

Plagioclase. Representative plagioclase analyses from cumulate and isotropic gabbros are shown in Table 3. As mentioned earlier, plagioclase of the plutonic suite has crystallized after olivine. Plagioclase shows a significant variation in anorthite content which correlates with the decrease in FeO/MgO in olivine and pyroxene. Its composition varies from an $An_{43.6}$ to $An_{77.7}$ type in cumulate gabbro and following a relatively more sodic trend of composition from $An_{42.6}$ to $An_{66.3}$ in isotropic gabbro. We link the compositional inhomogeneity of the plagioclase to changes in the composition of the liquid within the magma chamber. No zoning was detected in samples. Calcium-rich plagioclase characteristics of island-arc plutons in the cumulate sequence of the Troodos ophiolite (Ballantyne, 1992) is absent in the Bande-Zeyarat gabbros. Furthermore, numerous melting studies of primitive MORB (Green and Jaques, 1979; Bender et al., 1978; Hopper and Smith, 1996) indicate that the first crystallizing plagioclase is always < An_{85}. These finding together with the fact that plagioclase in mid-oceanic ridge gabbros are generally less calcic [i.e., mid-Atlantic Ridge (An_{72-88}), southwest Indian Ridge (An_{79-56})] (Hodges and Papike, 1976; Meyer et al., 1989) suggest that the Bande-Zeyarat gabbroic complex may have formed in a mid-oceanic ridge environment from a more evolved liquid.

Clinopyroxene. Table 4 and Fig. 5 show the data of the clinopyroxene analyses from cumulate and isotropic gabbros. In cumulate gabbro, clinopyroxene is seen as cumulus and intercumulus phase in either olivine gabbro or diopside-olivine gabbro. The clinopyroxenes from cumulate ($Fs_{8.38-15.98}En_{41.88-47.64}Wo_{42.27-55.36}$) and in isotropic gabbros ($Fs_{10.94-21.54}En_{39.29-47.03}Wo_{39.80-40}$) show limited compositional variations and plot mainly within the diopside-augite field of the pyroxene ternary diagram (Fig. 5c). The key to distinguish between clinopyroxenes in layered cumulate gabbro and isotropic gabbro is a relatively high Cr_2O_3, TiO_2, and low FeO contents in the former (Table 4). The unzoned nature and uniform composition of clinopyroxenes may indicate either subsolidus re-equilibration or a slow cooling, or both (Flower et al., 1977). High Si relative to tetrahedral Al in the Bande-Zeyarat clinopyroxenes also indicates derivation from a tholeiitic melt, based on the division of Kushiro (1960).

The Cr_2O_3 in clinopyroxenes is plotted against the Mg number in Fig. 6. A decrease in the amount of Cr_2O_3 is obvious by a decrease of Mg content. This relationship is interpreted by Elthon (1987) as a result of crystal fractionation of a basaltic liquid. In comparison to isotropic gabbro, most of the clinopyroxene of cumulate gabbro plot outside but close to the field of low-pressure clinopyroxene (Fig. 6), derived from 1 atm experimental studies of N-type MORB (Elthon, 1987). Experiments on oceanic basalts show that the most primitive clinopyroxenes that crystallize at 1 atm generally have Mg numbers less than 84 (Walker et al., 1979; Grove and Bryan, 1983). Using crystallization of the Mid-Cayman Rise glasses at 5 kbar, Elthon (1987) also reported clinopyroxenes with Mg numbers as high as 80. The

Table 2 - Representative olivine analyses from the Bande-Zeyarat gabbro complex.

Sample	CGQ46.4.1	CGQ46.6.1	CGQ46.6.2	CGQ46.7.1	CGQ46.10.1	CGQ61.11.1	CGQ61.11.2	CGQ61.12.1	CGQ61.14.1	CGQ61.14.2	CGQ61.15.2
Wt%											
SiO_2	37.08	36.95	37.29	36.76	36.95	37.64	37.56	37.42	37.74	37.92	37.76
TiO_2	b.d.	0.02	0.02	0.01	0.01	0.05	0.02	0.01	b.d.	0.03	0.03
FeO^*	24.53	25.81	25.15	25.61	25.32	20.75	20.52	20.60	20.63	20.66	20.74
MnO	0.35	0.35	0.37	0.41	0.39	0.30	0.32	0.32	0.28	0.31	0.30
MgO	37.16	36.37	36.70	35.98	36.31	40.20	40.26	39.96	39.96	40.00	39.75
CaO	0.01	b.d.	0.02	0.02	b.d.	0.01	b.d.	0.02	0.01	0.01	0.01
NiO	0.11	0.08	0.13	0.06	0.11	0.14	0.18	0.11	0.18	0.14	0.15
Total	99.24	99.58	99.68	98.85	99.09	99.09	98.86	98.44	98.80	99.07	98.74
Si	0.986	0.985	0.990	0.988	0.989	0.984	0.984	0.985	0.989	0.991	0.991
Ti	0.000	0.000	0.000	0.000	0.000	0.002	0.000	0.000	0.000	0.000	0.000
Fe	0.545	0.575	0.558	0.575	0.566	0.454	0.450	0.454	0.452	0.452	0.456
Mn	0.008	0.008	0.008	0.010	0.008	0.006	0.008	0.008	0.006	0.006	0.006
Mg	1.473	1.445	1.451	1.440	1.448	1.566	1.572	1.567	1.561	1.557	1.555
Ca	0.000	0.000	0.000	0.000	0.000	0.000	0.000	0.000	0.000	0.000	0.000
Ni	0.002	0.002	0.003	0.002	0.002	0.003	0.003	0.002	0.003	0.003	0.003
Total	3.014	3.015	3.010	3.015	3.013	3.015	3.017	3.016	3.011	3.009	3.011
Fo	72.77	71.29	72.14	71.29	71.78	77.72	77.72	77.61	77.61	77.61	77.50
Fa	27.23	28.71	27.86	28.71	28.22	22.28	22.28	22.39	22.39	22.39	22.50

Sample	CGQ61.15.c.1	CGQ61.9.1	CGQ61.9.2	CGQT59.1	CGQT59.1.1	CGQT59.3.1	CGQT59.4.1	CGQT59.5.1	IGQ1	IGQ2	IGQ3
Wt%											
SiO_2	37.62	37.58	37.60	37.10	38.01	37.77	37.58	37.90	36.15	35.75	36.71
TiO_2	0.04	0.02	0.04	0.03	0.01	0.02	0.04	0.02	0.02	0.01	0.01
FeO^*	20.66	21.32	21.06	20.08	20.43	20.05	19.94	20.37	28.95	33.55	28.20
MnO	0.29	0.34	0.31	0.31	0.30	0.32	0.27	0.30	0.44	0.68	0.44
MgO	39.56	39.46	39.60	41.52	40.20	40.30	40.84	40.56	33.75	30.50	34.77
CaO	0.02	0.01	0.02	0.02	0.01	0.02	0.01	0.02	0.03	0.04	0.01
NiO	0.18	0.15	0.15	0.09	0.19	0.16	0.19	0.13	0.05	0.06	0.03
Total	98.37	98.88	98.78	99.15	99.15	98.64	98.87	99.30	99.39	100.59	100.17
Si	0.991	0.987	0.988	0.969	0.992	0.989	0.981	0.987	0.982	0.981	0.985
Ti	0.002	0.000	0.002	0.000	0.000	0.000	0.002	0.000	0.000	0.000	0.000
Fe	0.456	0.469	0.462	0.438	0.445	0.439	0.436	0.444	0.657	0.770	0.632
Mn	0.006	0.008	0.006	0.006	0.006	0.008	0.006	0.006	0.010	0.016	0.010
Mg	1.552	1.546	1.550	1.617	1.561	1.572	1.589	1.573	1.365	1.247	1.390
Ca	0.000	0.000	0.000	0.000	0.000	0.000	0.000	0.000	0.002	0.002	0.000
Ni	0.003	0.003	0.003	0.002	0.005	0.003	0.005	0.003	0.002	0.002	0.000
Total	3.010	3.013	3.011	3.032	3.009	3.011	3.019	3.013	3.018	3.018	3.017
Fo	77.50	76.73	77.11	78.54	77.61	78.11	78.22	78.11	67.80	63.80	69.00
Fa	22.50	23.27	22.89	21.46	22.39	21.89	21.78	21.89	32.20	36.20	31.00

Number of ions on the basis of 4 (O), total Fe as FeO*. Abbreviations as in Table 1.

Table 3 - Representative plagioclase analyses from the Bande-Zeyarat gabbro complex.

Sample	CGQ15.1.1-1	CGQ15.1.1-3	CGQ15.6.1	CGQ.20.2.1-1	CGQ.20.2.1-2	CGQ.20.2.1-3	CGQ.20.3.1	CGQ38.1.1-1	CGQ38.1.1-3	CGQ38.2.1
Wt%										
SiO_2	50.70	50.34	52.60	56.27	55.89	56.82	56.17	48.96	48.29	52.31
Al_2O_3	30.38	30.70	29.44	27.64	27.44	27.82	28.17	32.44	32.07	30.18
FeO^*	0.09	0.19	0.15	0.11	0.13	0.14	0.28	0.16	0.30	0.28
MgO	b.d.	b.d.	0.01	b.d.	b.d.	b.d.	0.01	0.01	0.03	0.30
CaO	13.14	13.29	11.90	9.08	9.25	9.63	9.84	14.88	15.51	11.51
Na_2O	4.15	4.08	4.79	6.38	6.23	6.37	6.10	3.12	2.91	4.56
K_2O	0.09	0.07	0.09	0.11	0.16	0.15	0.13	0.04	0.02	0.24
Total	98.55	98.67	98.98	99.59	99.10	100.93	100.70	99.61	99.13	99.38
Si	4.681	4.646	4.813	5.071	5.067	5.062	5.027	4.495	4.464	4.768
Al^{IV}	1.319	1.354	1.187	0.929	0.933	0.938	0.973	1.505	1.536	1.232
Al^{VI}	1.986	1.983	1.992	2.008	1.998	1.983	1.994	2.002	1.962	2.009
Fe	0.006	0.017	0.011	0.011	0.011	0.011	0.022	0.011	0.022	0.022
Mg	0.000	0.000	0.000	0.000	0.000	0.000	0.000	0.000	0.006	0.038
Ca	1.298	1.314	1.166	0.878	0.899	0.920	0.941	1.461	1.538	1.122
Na	0.744	0.732	0.848	1.116	1.100	1.102	1.054	0.552	0.522	0.810
K	0.012	0.012	0.012	0.010	0.022	0.022	0.010	0.000	0.000	0.032
Total	10.046	10.058	10.029	10.023	10.030	10.038	10.021	10.026	10.050	10.033
Ab	35.90	35.30	41.60	55.40	54.50	53.90	52.50	27.70	25.20	41.20
An	63.10	64.70	57.40	43.60	44.60	45.10	46.50	72.30	74.80	57.70
Or	1.00	0.00	1.00	1.00	1.00	1.00	1.00	0.00	0.00	1.00

Table 3 *continue*

Sample	CGQ38.2.2	CGQ38.3.1-1	CGQ38.3.1-4	CGQ38.4.c.1	CGQ38.4.m.2	CGQ.42.3.1	CGQ46.5.1	CGQ46.5.2	CGQ46.6.1
Wt%									
SiO_2	48.85	49.15	49.24	48.60	48.35	48.93	50.18	50.82	50.49
Al_2O_3	32.18	32.53	32.42	32.18	32.15	32.64	31.31	31.18	31.55
FeO^*	0.82	0.22	0.22	0.18	0.31	0.22	0.26	0.20	0.24
MgO	0.04	0.02	0.07	0.02	0.03	b.d.	b.d.	0.02	b.d.
CaO	15.04	15.32	15.00	15.04	15.28	15.14	13.90	13.82	14.14
Na_2O	3.00	3.05	3.01	3.16	3.02	3.06	3.68	3.85	3.55
K_2O	0.04	0.05	0.08	0.03	0.05	0.02	0.05	0.04	0.05
Total	99.97	100.34	100.04	99.21	99.19	100.01	99.38	99.93	100.02
Si	4.482	4.484	4.497	4.482	4.470	4.476	4.603	4.635	4.603
Al^{IV}	1.518	1.516	1.503	1.518	1.530	1.524	1.397	1.365	1.397
Al^{VI}	1.966	1.981	1.989	1.983	1.968	1.995	1.988	1.988	1.989
Fe	0.061	0.016	0.016	0.017	0.022	0.016	0.022	0.016	0.016
Mg	0.006	0.000	0.011	0.000	0.006	0.000	0.000	0.000	0.000
Ca	1.477	1.496	1.466	1.485	1.510	1.484	1.367	1.348	1.381
Na	0.530	0.538	0.538	0.566	0.544	0.538	0.650	0.680	0.624
K	0.000	0.010	0.010	0.000	0.012	0.000	0.012	0.000	0.010
Total	10.040	10.041	10.030	10.051	10.062	10.033	10.039	10.032	10.020
Ab	26.70	26.50	27.00	27.50	26.20	26.70	32.70	33.30	31.00
An	73.30	73.50	73.00	72.50	73.80	73.30	67.30	66.70	69.00
Or	0.00	0.00	0.00	0.00	0.00	0.00	0.00	0.00	0.00

Sample	CGQ46.6.2	CGQ46.7.1	CGQ46.8.1	CGQ46.10.1	CGQ59.2.1	CGQ59.3.2	CGQ61.11.2	CGQ61.11.c.1	CGQ61.11.m.1	CGQ61.14.c.1
Wt%										
SiO_2	49.68	51.24	50.09	49.80	50.19	49.57	49.63	49.66	47.32	49.62
Al_2O_3	31.68	30.61	31.27	31.74	31.03	31.06	31.71	31.97	32.92	31.62
FeO^*	0.24	0.32	0.19	0.17	0.11	0.16	0.13	0.14	0.38	0.10
MgO	0.01	b.d.	b.d.	b.d.	0.01	b.d.	b.d.	b.d.	b.d.	b.d.
CaO	14.61	13.19	13.79	14.50	13.88	14.02	14.39	14.70	16.23	14.41
Na_2O	3.42	4.06	3.78	3.42	3.56	3.66	3.57	3.14	2.53	3.45
K_2O	0.06	0.06	0.04	0.03	0.10	0.10	0.04	0.04	0.03	0.05
Total	99.70	99.48	99.16	99.66	98.88	98.57	99.47	99.65	99.41	99.25
Si	4.552	4.687	4.603	4.563	4.623	4.588	4.554	4.543	4.375	4.562
Al^{IV}	1.448	1.313	1.397	1.437	1.377	1.412	1.446	1.457	1.625	1.438
Al^{VI}	1.975	1.984	1.992	1.986	1.989	1.980	1.983	1.997	1.966	1.586
Fe	0.017	0.022	0.017	0.011	0.011	0.011	0.011	0.011	0.028	0.006
Mg	0.000	0.000	0.000	0.000	0.000	0.000	0.000	0.000	0.000	0.000
Ca	1.437	1.291	1.358	1.426	1.373	1.390	1.417	1.441	1.607	1.419
Na	0.606	0.726	0.674	0.606	0.632	0.656	0.640	0.562	0.456	0.618
K	0.012	0.010	0.000	0.000	0.012	0.012	0.000	0.000	0.000	0.012
Total	10.047	10.033	10.041	10.029	10.017	10.049	10.051	10.011	10.057	10.041
Ab	29.40	35.60	33.30	29.70	31.70	31.70	31.10	28.00	22.30	30.40
An	70.60	64.40	66.70	70.30	67.30	67.30	68.90	72.00	77.70	69.60
Or	0.00	0.00	0.00	0.00	1.00	1.00	0.00	0.00	0.00	0.00

Sample	CGQ61.15.c.1	CGQ61.15.m.1	CGQ61.9.1	CGQ73.7.1	CGQ73.7.3	CGQ73.9.1	CGQ73.10.2	IGQ13.1.c.1	IGQ13.1.r.1	IGQ13.4.1	IGQ13.4.2
Wt%											
SiO_2	48.77	49.23	49.20	52.58	53.43	52.96	53.32	56.54	56.51	56.34	56.61
Al_2O_3	31.97	31.77	31.74	29.06	28.56	29.22	28.67	27.32	27.01	27.01	27.32
FeO^*	0.13	0.14	0.21	0.38	0.42	0.34	0.36	0.20	0.52	0.24	0.23
MgO	b.d.	0.01	b.d.	0.03	0.05	0.04	0.03	0.01	0.07	0.02	0.01
CaO	14.86	14.78	14.44	11.81	10.74	12.01	11.64	9.00	8.92	8.87	8.97
Na_2O	3.11	3.33	3.25	4.69	5.22	4.58	4.71	6.27	6.47	6.35	6.45
K_2O	0.05	0.05	0.04	0.15	0.26	0.16	0.14	0.19	0.20	0.18	0.23
Total	98.89	99.31	98.88	98.70	98.68	99.31	98.87	99.53	99.70	99.01	99.82
Si	4.505	4.527	4.546	4.828	4.899	4.829	4.881	5.100	5.101	5.112	5.097
Al^{IV}	1.495	1.473	1.454	1.172	1.101	1.171	1.119	0.900	0.899	0.888	0.903
Al^{VI}	1.989	1.976	1.998	1.973	1.984	1.975	1.973	2.005	1.977	2.001	1.997
Fe	0.011	0.011	0.017	0.028	0.033	0.027	0.028	0.016	0.038	0.016	0.016
Mg	0.000	0.000	0.000	0.006	0.006	0.005	0.006	0.000	0.011	0.000	0.000
Ca	1.470	1.459	1.426	1.164	1.058	1.173	1.144	0.867	0.863	0.861	0.866
Na	0.554	0.596	0.578	0.838	0.926	0.812	0.836	1.094	1.128	1.112	1.126
K	0.012	0.012	0.000	0.022	0.034	0.022	0.012	0.022	0.022	0.022	0.022
Total	10.036	10.054	10.019	10.031	10.041	10.014	9.999	10.004	10.039	10.012	10.027
Ab	27.50	29.10	29.00	41.60	45.50	40.00	42.00	55.60	56.40	56.00	56.00
An	72.50	70.90	71.00	57.40	52.50	59.00	57.00	43.40	42.60	43.00	43.00
Or	0.00	0.00	0.00	1.00	2.00	1.00	1.00	1.00	0.00	1.00	1.00

Table 3 *continue*

Sample	IGQ13.10.1	IGQ36.4.1	IGQ54.6.1-1	IGQ54.6.1-3	IGQ54.7.1-1	IGQ54.7.1-2	IGQ57.3.1	IGQ57.4.1
Wt%								
SiO_2	56.64	53.87	50.73	50.41	50.75	50.69	52.19	51.87
Al_2O_3	27.20	28.17	30.69	30.88	30.58	30.61	29.65	29.84
FeO^*	0.14	0.26	0.14	0.30	0.12	0.11	0.14	0.14
MgO	b.d.	0.02	0.02	0.02	b.d.	0.01	0.01	b.d.
CaO	9.14	10.98	13.38	13.50	12.90	13.42	12.22	12.48
Na_2O	6.27	5.23	3.84	3.81	4.08	3.77	4.69	4.50
K_2O	0.19	0.14	0.07	0.06	0.08	0.06	0.11	0.13
Total	99.58	98.67	98.87	98.98	98.47	98.67	99.01	98.96
Si	5.107	4.935	4.665	4.639	4.680	4.671	4.781	4.755
Al^{IV}	0.893	1.065	1.335	1.361	1.320	1.329	1.219	1.245
Al^{VI}	1.998	1.976	1.992	1.990	2.003	1.992	1.983	1.984
Fe	0.011	0.022	0.011	0.022	0.011	0.011	0.011	0.011
Mg	0.000	0.000	0.000	0.000	0.000	0.000	0.000	0.000
Ca	0.883	1.080	1.321	1.332	1.274	1.323	1.199	1.229
Na	1.094	0.926	0.686	0.674	0.732	0.676	0.836	0.804
K	0.022	0.012	0.012	0.012	0.012	0.012	0.012	0.012
Total	10.008	10.016	10.022	10.030	10.032	10.014	10.041	10.040
Ab	55.00	45.50	34.00	33.70	36.00	34.00	40.80	39.20
An	44.00	53.50	66.00	66.30	64.00	66.00	58.30	59.80
Or	1.00	1.00	0.00	0.00	0.00	0.00	1.00	1.00

Number of ions on the basis of 16 (O), total Fe as FeO*. Abbreviations as in Table 1.

Table 4 - Representative clinopyroxene analyses from the Bande-Zeyarat gabbro complex.

Sample	CGQ15.1.1	CGQ15.1.2	CGQ15.2.1	CGQ15.2.2	CGQ15.4.1	CGQ15.4.2	CGQ15.6.2	CGQ20.4.1	CGQ38.1.1	CGQ38.4.3	CGQ38.4.4
Wt%											
SiO_2	50.89	50.90	50.88	50.88	50.72	50.75	51.83	52.93	52.21	52.22	52.27
Al_2O_3	3.28	2.80	3.04	2.68	3.37	3.10	2.60	1.88	3.40	3.85	3.17
TiO_2	0.96	0.73	0.94	0.71	0.85	0.80	0.60	0.29	0.84	0.90	0.66
FeO^*	8.41	7.72	7.61	7.82	7.58	7.86	8.40	7.70	6.16	6.15	5.90
MnO	0.27	0.24	0.25	0.26	0.26	0.24	0.27	0.32	0.24	0.21	0.21
MgO	14.50	14.48	14.70	14.42	14.47	14.08	14.57	15.04	14.95	14.68	15.25
Cr_2O_3	0.05	0.09	0.05	0.04	0.21	0.06	0.08	0.35	0.39	0.27	0.23
CaO	21.29	22.01	21.60	21.89	21.04	21.67	21.55	22.36	23.07	22.40	22.93
Na_2O	0.38	0.38	0.41	0.37	0.55	0.40	0.40	0.43	0.47	0.41	0.37
Total	100.03	99.35	99.48	99.07	99.05	98.96	100.30	100.98	101.73	101.09	100.99
Si	1.898	1.914	1.898	1.914	1.908	1.910	1.916	1.947	1.895	1.903	1.914
Al^{IV}	0.102	0.086	0.102	0.086	0.092	0.090	0.084	0.053	0.105	0.097	0.086
Al^{VI}	0.041	0.036	0.033	0.031	0.057	0.045	0.031	0.026	0.039	0.070	0.051
Ti	0.027	0.021	0.027	0.021	0.025	0.023	0.018	0.009	0.024	0.024	0.018
Fe	0.262	0.242	0.237	0.246	0.237	0.246	0.260	0.236	0.187	0.188	0.180
Mn	0.009	0.007	0.009	0.009	0.009	0.007	0.009	0.011	0.007	0.007	0.007
Mg	0.806	0.811	0.818	0.809	0.811	0.789	0.801	0.824	0.809	0.797	0.832
Cr	0.000	0.005	0.000	0.000	0.005	0.000	0.005	0.009	0.013	0.009	0.009
Ca	0.851	0.886	0.862	0.881	0.847	0.872	0.852	0.882	0.896	0.874	0.900
Na	0.020	0.020	0.040	0.020	0.040	0.020	0.020	0.040	0.040	0.040	0.020
Total	4.016	4.028	4.026	4.017	4.031	4.002	3.996	4.037	4.015	4.009	4.017
Fs	13.61	12.44	12.5	12.89	12.70	13.09	13.47	12.37	10.00	10.16	9.42
En	41.88	41.97	42.71	41.75	42.85	41.36	41.97	42.27	42.63	42.78	43.46
Wo	44.50	45.60	44.79	45.36	44.45	45.55	44.56	55.36	47.37	47.06	47.12
Mg#	75.47	77.02	77.54	76.68	77.39	76.23	75.49	77.74	81.22	80.91	82.21

Sample	CGQ46.10.1	CGQ46.2.1	CGQ46.2.2	CGQ46.4.1	CGQ46.7.2	CGQ46.8.2	CGQ46.9.1	CGQ46.9.2	CGQ59.5.1	CGQ59.5.2	CGQ61.14.2
Wt%											
SiO_2	51.99	51.31	51.19	51.93	52.01	51.97	51.78	51.61	51.77	51.84	51.22
Al_2O_3	2.85	3.53	3.12	3.41	3.22	3.33	3.34	3.16	3.13	3.05	3.14
TiO_2	0.61	0.83	0.73	0.83	0.80	0.82	0.82	0.86	0.84	0.83	0.71
FeO^*	6.73	6.57	6.33	6.15	7.10	6.94	6.92	7.29	5.77	5.90	6.21
MnO	0.21	0.16	0.17	0.22	0.22	0.25	0.21	0.24	0.16	0.16	0.16
MgO	15.47	15.04	15.45	15.32	15.64	15.75	15.73	15.68	16.16	16.13	16.45
Cr_2O_3	0.20	0.24	0.19	0.24	0.21	0.21	0.21	0.14	0.4	0.38	0.49
CaO	22.20	22.54	22.52	22.62	21.19	21.39	21.32	21.54	21.96	21.78	20.27
Na_2O	0.37	0.47	0.45	0.42	0.42	0.45	0.4	0.37	0.42	0.40	0.42
Total	100.63	100.69	100.15	101.14	100.81	101.11	100.73	100.89	100.61	100.47	99.07
Si	1.912	1.888	1.892	1.901	1.905	1.903	1.905	1.899	1.901	1.907	1.900
Al^{IV}	0.088	0.112	0.108	0.099	0.095	0.097	0.095	0.101	0.099	0.093	0.100
Al^{VI}	0.036	0.043	0.029	0.046	0.046	0.048	0.051	0.036	0.038	0.040	0.038
Ti	0.018	0.022	0.020	0.022	0.022	0.022	0.022	0.025	0.022	0.022	0.020
Fe	0.208	0.201	0.195	0.189	0.218	0.213	0.212	0.223	0.286	0.181	0.192
Mn	0.007	0.004	0.004	0.007	0.007	0.009	0.007	0.007	0.007	0.004	0.004
Mg	0.849	0.824	0.850	0.836	0.854	0.860	0.862	0.860	0.841	0.884	0.910
Cr	0.005	0.009	0.005	0.009	0.005	0.005	0.005	0.005	0.005	0.009	0.013
Ca	0.875	0.888	0.892	0.887	0.832	0.838	0.840	0.849	0.784	0.857	0.805
Na	0.020	0.040	0.040	0.040	0.040	0.040	0.020	0.020	0.020	0.020	0.040
Total	4.018	4.031	4.035	4.036	4.024	4.035	4.019	4.025	4.003	4.017	4.022
Fs	10.88	10.47	10.31	9.95	11.58	10.99	10.99	14.4	9.38	9.38	9.95
En	44.04	42.93	43.81	43.46	44.74	45.03	45.03	44.56	45.83	45.83	47.64
Wo	45.08	46.60	45.88	46.60	43.68	43.98	43.98	44.04	44.79	44.79	42.41
Mg#	80.32	80.39	81.34	81.56	79.66	80.15	80.26	79.41	83.36	83.00	82.58

Table 4 *continue*

Sample	CGQ61.6.1	CGQ61.6.2	CGQ61.6.3	CGQ61.6.4	CGQ61.8.1	CGQ61.8.2	CGQ73.9.1	IGQ13.1	IGQ13.5.1	IGQ36.2.c.1
Wt%										
SiO_2	52.42	52.35	51.05	52.78	52.19	52.13	51.21	52.05	52.92	50.26
Al_2O_3	3.24	3.28	3.26	2.80	3.07	3.16	2.31	1.48	1.27	3.42
TiO_2	0.71	0.60	0.79	0.59	0.72	0.74	0.99	0.37	0.29	1.01
FeO*	5.27	5.43	6.86	5.61	5.19	5.40	10.06	13.14	13.64	8.39
MnO	0.19	0.21	0.21	0.15	0.15	0.19	0.47	0.39	0.40	0.17
MgO	15.71	15.71	15.31	16.04	15.63	15.74	14.61	13.85	13.78	14.86
Cr_2O_3	0.41	0.59	0.79	0.34	0.49	0.48	0.01	0.01	0.01	0.01
CaO	23.05	22.36	22.25	22.88	22.46	22.33	20.41	19.42	19.34	20.28
Na_2O	0.51	0.51	0.47	0.44	0.51	0.47	0.32	0.32	0.29	0.37
Total	101.51	101.04	100.99	101.63	100.41	100.64	100.49	101.03	101.94	98.77
Si	1.901	1.908	1.879	1.914	1.912	1.910	1.909	1.949	1.965	1.890
Al^{IV}	0.099	0.092	0.121	0.086	0.088	0.090	0.091	0.051	0.035	0.110
Al^{VI}	0.040	0.048	0.020	0.032	0.044	0.047	0.012	0.016	0.018	0.044
Ti	0.020	0.018	0.022	0.016	0.020	0.020	0.027	0.012	0.009	0.030
Fe	0.159	0.166	0.210	0.170	0.158	0.165	0.314	0.412	0.424	0.264
Mn	0.007	0.007	0.007	0.004	0.004	0.007	0.016	0.011	0.013	0.005
Mg	0.850	0.854	0.840	0.868	0.854	0.858	0.811	0.774	0.763	0.834
Cr	0.013	0.017	0.022	0.009	0.013	0.013	0.000	0.000	0.000	0.000
Ca	0.896	0.874	0.877	0.889	0.880	0.876	0.815	0.779	0.769	0.818
Na	0.040	0.040	0.040	0.040	0.040	0.040	0.020	0.020	0.020	0.020
Total	4.025	4.024	4.038	4.028	4.013	4.026	4.015	4.024	4.016	4.015
Fs	8.38	8.95	10.88	8.81	8.47	8.90	15.98	20.92	21.54	13.61
En	44.50	44.21	43.52	45.08	44.97	45.03	41.75	39.29	38.97	43.46
Wo	47.12	46.84	45.60	46.11	46.56	46.07	42.27	39.80	39.49	42.93
Mg#	84.24	83.73	80.00	83.62	84.39	83.87	72.09	65.26	64.28	75.96

Sample	IGQ36.4.1	IGQ54.5.1	IGQ54.5.2	IGQ54.5.3	IGQ54.5.4	IGQ54.7.1	IGQ54.7.2	IGQ54.9.c.1	IGQ54.9.m.1	IGQ57.2.1	IGQ57.2.2	IGQ57.5.1
Wt%												
SiO_2	51.39	51.43	51.22	51.36	52.28	51.34	50.80	52.12	51.78	51.63	49.92	51.47
Al_2O_3	2.79	3.20	3.44	3.20	3.09	3.53	3.43	2.93	2.90	2.90	3.02	3.34
TiO_2	0.96	0.77	0.67	0.63	0.57	0.54	0.86	0.63	0.67	0.79	0.85	0.80
FeO*	8.00	9.28	8.03	8.05	7.76	7.80	7.46	8.48	7.40	7.12	7.01	7.05
MnO	0.16	0.23	0.24	0.20	0.17	0.21	0.26	0.23	0.22	0.20	0.20	0.21
MgO	15.25	15.30	14.38	14.50	15.71	14.59	14.13	14.58	14.24	14.52	14.61	14.60
Cr_2O_3	0.04	0.18	0.17	0.17	0.10	0.20	0.14	0.08	0.06	0.16	0.18	0.44
CaO	21.23	19.80	21.33	21.19	18.55	21.16	22.49	20.48	22.50	22.57	22.71	21.98
Na_2O	0.38	0.37	0.42	0.45	0.34	0.44	0.51	0.42	0.42	0.48	0.51	0.54
Total	100.20	100.56	99.90	99.75	98.57	99.81	100.08	99.95	100.19	100.37	99.01	100.43
Si	1.907	1.901	1.909	1.915	1.949	1.905	1.893	1.925	1.923	1.907	1.878	1.894
Al^{IV}	0.093	0.099	0.091	0.085	0.051	0.095	0.107	0.075	0.077	0.093	0.122	0.106
Al^{VI}	0.028	0.038	0.061	0.054	0.084	0.061	0.045	0.054	0.048	0.031	0.013	0.040
Ti	0.027	0.022	0.018	0.018	0.016	0.016	0.025	0.018	0.018	0.022	0.025	0.022
Fe	0.248	0.286	0.251	0.251	0.242	0.243	0.233	0.262	0.230	0.220	0.221	0.217
Mn	0.004	0.007	0.007	0.007	0.004	0.007	0.009	0.007	0.007	0.007	0.007	0.007
Mg	0.843	0.841	0.800	0.806	0.874	0.807	0.784	0.804	0.787	0.799	0.818	0.800
Cr	0.000	0.005	0.005	0.005	0.005	0.005	0.005	0.005	0.000	0.005	0.005	0.013
Ca	0.845	0.784	0.851	0.847	0.741	0.841	0.898	0.810	0.894	0.892	0.915	0.866
Na	0.020	0.020	0.040	0.040	0.020	0.040	0.040	0.040	0.040	0.040	0.040	0.040
Total	4.015	4.003	4.033	4.028	3.986	4.020	4.039	4.000	4.024	4.016	4.044	4.005
Fs	12.95	15.18	13.16	13.16	12.97	12.70	12.04	13.83	12.04	11.52	11.22	11.64
En	43.52	43.98	42.11	42.11	47.03	42.86	40.84	43.09	41.36	41.88	41.84	42.33
Wo	43.52	40.84	44.74	44.74	40.00	44.44	47.12	43.09	46.60	46.60	46.94	46.03
Mg#	77.27	74.62	76.12	76.25	78.32	76.86	77.09	75.42	77.38	78.41	78.73	78.66

Sample	IGQ57.5.2	IGQ57.5.3	IGQ57.5.4	IGQ57.5.6
Wt%				
SiO_2	52.21	52.43	51.90	52.11
Al_2O_3	2.76	2.86	3.05	2.62
TiO_2	0.70	0.75	0.73	0.66
FeO*	6.80	7.05	6.75	7.26
MnO	0.21	0.21	0.19	0.23
MgO	14.92	14.31	14.84	14.40
Cr_2O_3	0.02	0.28	0.34	0.16
CaO	22.73	22.90	22.08	22.85
Na_2O	0.45	0.45	0.51	0.44
Total	100.80	101.24	100.39	100.73
Si	1.921	1.921	1.910	1.916
Al^{IV}	0.079	0.079	0.090	0.084
Al^{VI}	0.040	0.044	0.043	0.031
Ti	0.020	0.020	0.020	0.018
Fe	0.210	0.216	0.208	0.223
Mn	0.007	0.007	0.007	0.007
Mg	0.818	0.781	0.813	0.789
Cr	0.000	0.009	0.009	0.005
Ca	0.895	0.898	0.871	0.899
Na	0.040	0.040	0.040	0.040
Total	4.030	4.015	4.011	4.012
Fs	10.94	11.58	11.05	11.52
En	42.71	41.05	43.16	41.36
Wo	46.35	47.37	45.79	47.12
Mg#	79.57	78.34	79.63	77.96

Number of ions on the basis of 6 (O), total Fe as FeO*. Abbreviations as in Table 1.

clinopyroxenes in the Bande-Zeyarat gabbroic complex have Mg numbers 72.32-84.16 in cumulate, and 64.40-79.16 in isotropic gabbros, which may suggest crystallization in a low to moderate pressure environment which is also shown in Fig. 6.

Elthon (1987) suggested that clinopyroxenes formed either at a moderate or higher pressure, also have high Al_2O_3 (> 3%) and TiO_2 (> 1%) contents. The clinopyroxene data from the Kahnuj Bande-Zeyarat gabbros are presented by Al_2O_3 = 1.88-3.85%, TiO_2 = 0.29-0.99% in cumulate gabbro, and Al_2O_3 = 1.27-3.43%, TiO_2 = 0.29-1.01% in isotropic gabbro. The Al_2O_3 and TiO_2 contents of clinopyroxenes are plotted in Fig. 7, where they fall in low and moderate pressure fields. This is congruent with the results shown in Fig. 6.

Experimental data (Grove and Bryan, 1983) show that the equilibrium distribution coefficients for TiO_2 between clinopyroxene and basaltic liquids range from 0.25 to 0.35 at 1 atm pressure and could be as high as 0.75 at high pressure (10-25 kbar) (Bender et al., 1978; Elthon and Scrafe, 1984). These and other experiments (Kushiro and Yoder, 1965; 1966; Herzberg, 1978; Gasparik, 1984) also indicate that solubility of Al_2O_3 increases in clinopyroxene at higher temperature or pressure. So in regards to Al_2O_3 and TiO_2 contents we may also conclude that clinopyroxene crystallized at low to moderate pressure (5-10 kbar). Elthon (1987) believes that the pressure of crystallization in MORB petrogenesis is a variable factor; that means that different rock types may form at various pressure levels.

Chemical compositions of olivine, plagioclase and clinopyroxene follow zig-zag cryptic patterns throughout the gabbro sequence (Kananian et al., 2001). This clearly indicates replenishment of the magma chamber by influxes of a primitive melt during its crystallization process. The consequence of each episodic cryptic layering is to reset the Fo percentage in olivine, Mg numbers in clinopyroxene, and An percentage in plagioclase to higher values. Thus, one cannot establish a clear evolutionary relationship between cumulate and isotropic gabbros.

DISCUSSION AND CONCLUSION

The Bande-Zeyarat gabbroic complex shows a mid-ocean ridge affinity. This claim is based on: (a) TiO_2 vs. $FeO_t/(FeO_t + MgO)$ fractionation trends which are indistinguishable from MORB, (b) olivine-plagioclase-clinopyroxene as main order of appearance of cumulus phase in the gabbroic complex which result in accumulation of large amounts of olivine gabbros and fewer troctolites and gabbronorites; and (c) presence of gabbros rich in Fe.

Fractional crystallization of the gabbro took place during tectonic deformation in an ocean floor type of environment. The deformation is represented by folded magmatic foliation, boudins, and thinning of the layers.

The gabbroic complex represents a complete tholeiitic intrusion controlled by fractional crystallization and accumulation. The cumulate rocks of the Bande-Zeyarat are primarily of adcumulus origin, characterized by unzoned cumulus minerals. The presence of anorthosites and troctolite layers indicates that plagioclase was an early crystallizing phase.

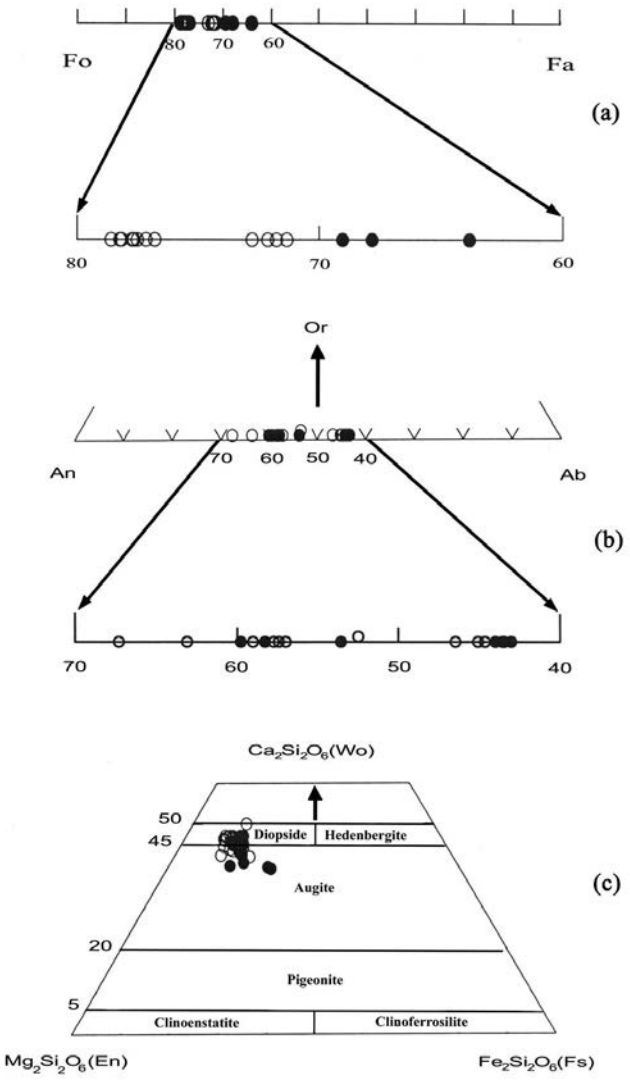

Fig. 5 - Chemical compositions of olivine (a), plagioclase (b) and clinopyroxene (c) in the Bande-Zeyarat gabbro complex. See Fig. 2 for key to symbols.

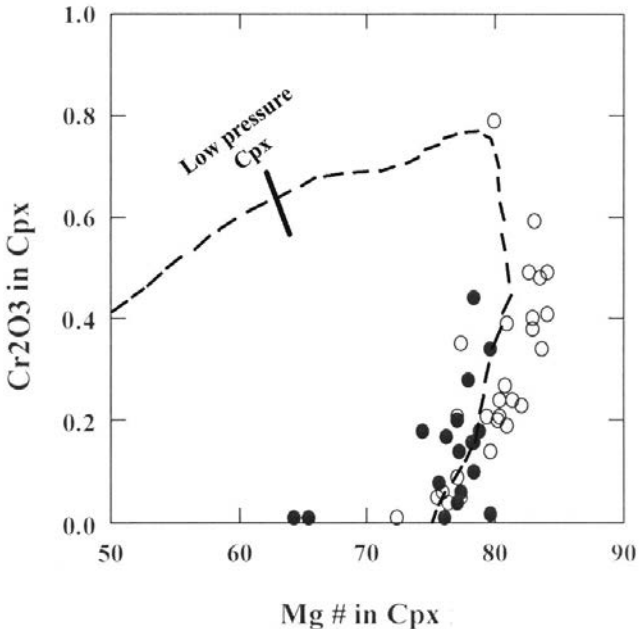

Fig. 6 - The Mg-number versus Cr_2O_3 in clinopyroxenes from the Bande-Zeyarat gabbro complex. Low-pressure clinopyroxene field from 1 atm experimental studies of N-MORB (Elthon, 1987). See Fig. 2 for key to symbols.

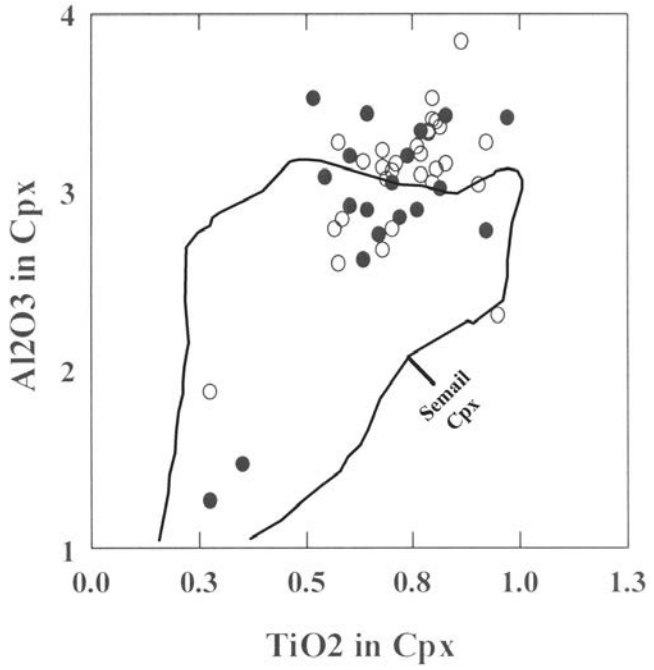

Fig. 7 - The TiO_2 versus Al_2O_3 contents of clinopyroxenes from the Bande-Zeyarat gabbro complex. The field of the Semail ophiolite is from Pallister and Hopson (1981). See Fig. 2 for key to symbols.

The low-level gabbro is "cumulate", in the sense that it crystallized from a larger mass of magma which entered the crust, cooled and partially crystallized. The isotropic gabbros did not form from cooling of remaining liquids extracted after cumulate formation, since they do not show any strong negative Eu anomalies. Thus it is hard to hypothesize fractional crystallization relationships between the two gabbro types, but they may have been generated from different batches of primary melts. In terms of composition and texture, high-level gabbros are generally coarse-grained, slowly cooled equivalents of sheeted dykes. In these and other aspects, the Bande-Zeyarat high-level gabbro is similar to shallow-level gabbro formed at the East Pacific Rise (Dick and Natland, 1996; Natland and Dick, 1996).

In the Bande-Zeyarat plutonic complex, the high-level and low-level gabbros are compositionally and texturally distinct. The cumulate gabbro is depleted in Zr and Y relative to N-MORB (Zr = 74, Y = 25), which indicates depletion of the magmas parental to the gabbro cumulates. The high-level gabbros have REE abundances and slope similar to sheeted dykes and lavas in the Kahnuj ophiolitic complex (Arvin et al., 2001). They have relatively higher SiO_2 content (*av*. 48.55) and high FeO* (*av*. 10.52) and TiO_2 (*av*. 1.80) concentrations compared to cumulate gabbro. The compositional diversity of the isotropic gabbro is explained if this rock mass was subjected to a high degree of fractionation and accumulation of both iron and titanium. Compared with the cumulate gabbro, the plagioclase and clinopyroxene in isotropic gabbro are relatively more albite-rich and iron-rich, respectively. The olivine is no longer a cumulate phase, and the isotropic gabbro is enriched in incompatible elements such as Zr, Y, Nb and REEs. Accordingly, it is apparent that high-level gabbros retained a relatively large proportion of trapped liquid, and/ or crystallized from a more evolved liquid, compared to lower gabbros.

Mineral assemblages, mineral chemistry (i.e., $Fo_{67.8\text{-}78.54}$, low Mg# < 84.16 and high Si relative to tetrahedral Al in clinopyroxenes), crystallization order (olivine-plagioclase-clinopyroxene-orthopyroxene-hornblende) and whole rock chemistry suggest that the Bande-Zeyarat gabbroic complex formed by low to moderate pressure crystal fractionation from a tholeiitic basaltic magma similar to MORB. In fact, most cumulate rocks formed by crystal fractionation of MORBs at moderate pressure would be mixtures of olivine, plagioclase and clinopyroxene (Elthon, 1987). Further support for a mid-oceanic origin of the Bande-Zeyarat gabbroic complex is given by its lack of calcium-rich plagioclase which is characteristic of island-arc plutons.

Based on the major, trace and REE elements geochemistry, as well as the mineral chemistry of the gabbroic complex, we suggest that the Kahnuj ophiolite represents a remnant of oceanic crust originated in a region analogous to a mid-ocean ridge and evolved to an off-axis environment. Thus, the Kahnuj ophiolite complex may represent an oceanic basin developed in the Mesozoic between the Lut block of Central Iran, and the Bajgan-Dur-Kan microcontinents.

Acknowledgements

We thank Prof. E. Saccani and anonymous reviewer for insightful comments that improved the manuscript. M. Arvin is greatly indebted to Prof. Sherman Bloomer, former Head of the Geology Department of Oregon State University, for facilitating and financial support of the analytical work.

REFERENCES

Arvin M., Houseinipour A., Babaei A. and Babaei H.S., 2001. Geochemistry and tectonic significance of basalts in the Dare-Anar complex: evidence from the Kahnuj ophiolitic complex, southeastern, Iran. J. Sci. I. R. Iran, 12: 157-170.

Ballantyne P., 1992. Petrology and geochemistry of the plutonic rocks of the Halmahera ophiolite, eastern Indonesia, an analogue of modern oceanic forearcs, In: L.M. Parson, B.J. Murton and P. Browning (Eds.), Ophiolites and their modern oceanic analogues, Geol. Soc. London Spec. Publ., 60: 179-202.

Barling J., Hertogen J. and Weis D., 1997. Whole-rock geochemistry and Sr-, Nd-, and Pb-isotopic characteristics of undeformed, deformed, and recrystallized gabbros from site 921, 922, and 923 in the Mark Area. ODP Sci. Results, 153: 351-362.

Beard J.S., 1986. Characteristic mineralogy of arc-related cumulate gabbros: implications for the tectonic setting of gabbroic plutons and for andesite genesis. Geology, 14: 848-851.

Bébien J., 1972. Teneurs en TiO_2 des roches volcaniques: comparaison des volcanismes actual et ophiolitique. C. R. Acad. Sci. Paris, 275D: 1967-1970.

Beccaluva L., Ohnenstetter D. and Ohnenstetter M., 1979. Geochemical discrimination between ocean floor and island-arc tholeiites-application to some ophiolites. Can. J. Earth Sci., 16: 1874-1882.

Bender J. F., Hodges F.N. and Bence A.E., 1978. Petrogenesis of basalts from the project famous area: experimental study from 0 to15 kbar. Earth Planet. Sci. Lett., 41: 277-302.

Berberian M. and King G.C.P., 1981. Towards a palaeogeography and tectonic evolution of Iran. Can. J. Earth Sci., 18: 210-265.

Coleman R.G., 1977. Ophiolites - Ancient oceanic lithosphere? Springer Verlag, Mineral and Rocks, 12, 229 pp.

Dick H.J.B. and Nathland J.H., 1996. Late stage melt evolution and transport in the shallow mantle beneath the East Pacific Rise. ODP Sci. Results, 147: 103-134.

Elthon D., 1987. Petrology of the gabbroic rocks from the Mid-Canyman rise spreading center. J. Geophys. Res., 92: 658-682.

Elthon D. and Scarfe C.M., 1984. High-pressure phase equilibria of a high-magnesia basalt and the genesis of primary oceanic basalts. Am. Mineral., 69: 1-15.

Flower M.F.J., Robinson P.T., Schmincke H.U. and Ohnmacht W., 1977. Magma fractionation systems beneath the Mid-Atlantic ridge at 36-37°N. Contrib. Mineral. Petrol., 64: 167-195.

Gasparik T., 1984. Two pyroxene thermobarometry with new experimental data in the system CaO-MgO-Al_2O_3-SiO_2. Contrib. Mineral. Petrol., 87: 87-94.

Gass I.G. and Smewing J.D., 1973. Intrusion, extrusion and metamorphism at constructive margins: Evidence from the Troodos Massif, Cyprus. Nature, 242: 26-29.

Ghadami Gh., Arvin M. and Hosseini S.Z., 2003. Study of fractionation and tectonic setting of Bande-Zeyarat complex in Kahnuj ophiolite, southeast of Kerman, Iran. Iranian 6th Geol. Congr. Abstr., p. 135-140 (in Persian).

Ghazi A.M., Hassanipak A.A., Mahoney J.J. and Duncan R.A., 2004. Geochemical characteristics, ^{40}Ar-^{39}Ar ages and original tectonic setting of the Bande-Zeyarat/Dar Anar ophiolite, Makran accretionary Prism, S.E. Iran. Tectonophysics, 393: 175-196.

Govindaraju K. and Mevelle G., 1987. Fully automated dissolution and separation methods for inductively coupled plasma atomic emission spectrometry rocks analysis. Application to the determination of rare earth elements. J. Analyt. Atomic Spectrum., 2: 615-621.

Green D.H. and Jaques A.L., 1979. Petrogenesis of mid-ocean ridge basalts. In: M.W. McElhinny (Ed.), The earth: its origin, structure and evolution. London, Academic Press, p. 265-295.

Grove T.L. and Bryan W.B., 1983. Fractionation of pyroxene-phyric MORB at low pressure: an experimental study. Contrib. Mineral. Petrol., 84: 293-309.

Hassanipak A.A., Ghazi A.M. and Wampler J.M., 1996. Rare earth element characteristics and K-Ar ages of the Bande-Zeyarat ophiolite complex, southeastern Iran. Can. J. Earth Sci., 33: 1534-1542.

Hebert R., Bideau D. and Hekinian R., 1983. Ultramafic and mafic rocks from the Garrett transform fault near 13 degrees 30's on the East Pacific Rise: Igneous petrology. Earth Planet. Sci. Lett., 65: 107-125.

Herzberg C., 1978. Pyroxene geothermometry and geobarometry: Experimental and thermodynamic evaluation of some subsolidus phase relations involving pyroxenes in the system CaO-MgO-Al_2O_3-SiO_2. Geochim. Cosmochim. Acta., 42: 945-957.

Hodges F.N. and Papike J.J., 1976. Magmatic cumulates from oceanic layer 3. J. Geophys. Res., 81: 4135-4151.

Hopper D.J. and Smith L.M., 1996. Petrology of the gabbro and sheeted basaltic intrusives at North Cape, New Zealand. New Zealand. J. Geol. Geophys., 39: 389-402.

Kananian A., Juteau T., Bellon H., Darvishzadeh A., Sabzehi M., Whitechurch H. and Ricou L.E., 2001. The ophiolite massif of Kahnuj (western Makran, southern Iran): new geological and geochronological data. C.R. Acad. Sci. Paris, Sci. Terre Plan., 332: 543-552.

Kelemen P.B., Koga K. and Shimizu N., 1997. Geochemistry of gabbro sills in the crust-mantle transition zone of the Oman ophiolite: implications for the origin of the oceanic lower crust. Earth Planet. Sci. Letts., 146: 475-488.

Knipper A., Ricou L.E. and Dercourt J., 1986. Ophiolites as indicators of the geodynamic evolution of the Tethyan ocean. Tectonophysics, 123: 213-240.

Kushiro I., 1960. Si-Al relations in clinopyroxenes from igneous rocks. Am. J. Sci., 258: 548-554.

Kushiro I. and Yoder H.S.Jr., 1965. The reactions between forsterite and anorthite at high pressure. Year Book Carnegie Inst. Washington, 64: 89-94.

Kushiro I. and Yoder H.S., 1966. Anorthite-forsterite and anorthite-enstatite reactions and their bearing on the basalt-eclogite transformation. J. Petrol., 7: 337-362.

Kuno H., 1968. Differentiation of basalt magmas. In: H. H. Hess and A. Poldervaart (Eds.), Basalts. John Wiley and Sons, 2: 623-688.

Lipin B.R. and McKay G.A., 1989. Geochemistry and mineralogy of rare earth elements. Mineral. Soc. Am. Rev. Mineral., 21.

McCall G.J.H. and Kidd R.G.W., 1981. The Makran, southeastern Iran: the anatomy of a convergent plate margin active from Cretaceous to present, In: J. Legett (Ed.), Trench-fore arc geology. Geol. Soc. London Spec. Publ., 10: 387-397.

McCall G.J.H., 1985. Explanatory text of the Minab quadrangle map: 1:250000, No. J13. Geol. Surv. Iran, Tehran, 530 pp.

McCall G.J.H., 1997. The geotectonic history of the Makran and adjacent areas of southern Iran. J. Asian Earth Sci., 15: 517-531.

Meyer P.S., Dick H.J.B. and Thompson G., 1989. Cumulate gabbros from the Southwest Indian Ridge, 54°S-7°16'E: implications for magmatic processes at slow spreading ridge. Contrib. Mineral. Petrol., 103: 44-63.

Moores E.M., 1982. Origin and emplacement of ophiolites. Rev. Geophys. Space Phys., 20: 735-760.

Moores E.M., Kellogg H. and Dilek Y., 2000. Tethyan ophiolites, mantle convection, and tectonic "historical contingency": A resolution of the "ophiolite conundrum". Geol. Soc. Am. Spec. Paper, 349: 3-12.

Nathland J. and Dick H.J.B., 1996. Melt migration through high-level gabbroic cumulates of the East Pacific Rise at Hess Deep: Interference from rock textures and mineral compositions. ODP Sci. Results, 147: 21-58.

Pallister J.S. and Hopson C. A., 1981. Semail ophiolite plutonic suite: Field relation, phase variation, cryptic variation and layering, and a model of a spreading ridge magma chamber. J. Geophys. Res., 86: 2593-2644.

Pallister J.S. and Knight R.J., 1981. Rare earth element geochemistry of the Semail ophiolite near Ibra, Oman. J. Geophys. Res., 86: 2673-2697.

Parlak O., Höck V. and Delaloye M., 2000. Supra-subduction zone origin of Pozantı-Karsantı ophiolite (southern Turkey) deduced from whole-rock and mineral chemistry of the gabbroic cumulates In: E. Bozkurt, J.A. Winchester and J.D.A. Piper (Eds.), Tectonic and magmatism in Turkey and the surrounding area. Geol. Soc. London Spec. Publ., 173: 219-234.

Parlak O., Höck V. and Delaloye M., 2002. The supra-subduction zone Pozantı-Karsantı ophiolite southern Turkey: Evidence for high pressure crystal fractionation of ultramafic cumulates. Lithos, 65: 205-224.

Ricou L.E., 1971. Le croissant ophiolitique Peri-Arabe: un ceinture de nappes mise en place au Cretace superieur. Rév. Géogr. Phys. Géol. Dyn., 13: 372-350.

Robertson A.H.F., 2002. Overview of the genesis and emplacement of Mesozoic ophiolites in the Eastern Mediterranean Tethyan region. Lithos, 65: 1-67.

Sabzehi M., Eshraghi S., Roshanravan J. and Ghiyasi M., 1993. Geology and mineral resources of titanium oxide mineral in Bande-Zeyarat ophiolites. Kavoshgaran Counsulting Engineers, Int. Rep., Iranian Minstery of Mine, 199 pp. (in Persian).

Sengor A.M.C., 1987. Tectonic of the Tethysides: orogeneic collage development in collisional setting. Ann. Rev. Earth Planet. Sci., 15: 213-244.

Sengor A.M.C., 1990. A new model for the Late Paleozoic-Mesozoic tectonic evolution of Iran and implications for Oman. Geol. Soc. London Spec. Publ., 49: 797-831.

Serri G., 1981. The petrochemistry of ophiolite gabbroic complexes: A key for the classification of ophiolites into Low-Ti and High-Ti types. Earth Planet. Sci. Lett., 52: 203-212.

Stakes D.S., Shervais J.W. and Hopson C.A., 1984. The volcanic tectonic cycle of the FAMOUS and AMAR vallys, Mid-Atlantic Ridge (36°47'N): Evidence from basalt glass and phenocryst compositional variations for a study state magma chamber beneath the valley midsections, AMAR 3. J. Geophys. Res., 89: 6995-7028.

Sun S.S. and McDonough W.F., 1989. Chemical and isotopic systematics of oceanic basalts: implications for mantle composition and processes. In: A.D. Saunder and M.J. Norry (Eds.), Magmatism in ocean basins. Geol. Soc. London Spec. Publ., 42: 313-345.

Tirrul R., Bell I.R., Griffs R.J. and Camp V.E., 1983. The Sistan Suture zone of eastern Iran. Bull. Geol. Soc. Am., 94: 134-150.

Vanko D.A. and Batiza R., 1982. Gabbroic rocks from the Mathematician Ridge failed rift. Nature, 300: 742-744.

Voldet P., 1993. From neutron activation to inductively coupled plasma-atomic emission spectrometry in the determination of rare-earth elements in rocks. Trends Analyt. Chemst., 12: 339-344.

Walker D., Shibata T. and Delong S.E., 1979. Abyssal tholeiites from the oceanographer fracture zone, II, phase equilibria and mixing. Contrib. Mineral. Petrol., 70: 111-126.

Winchester J.A. and Floyd P.A., 1977. Geochemical discrimination of different magma series and their differentiation products using immobile elements. Chem. Geol., 20: 325-343.

Xie Q., Kerrich R. and Fan J., 1993. HFSE/REE fractionation recorded in three komatiite-basalt sequences, Archean Abitibi greenstone belt: implications for multiple plume sources and depths. Geochim. Cosmochim. Acta, 57: 4111-4118.

Xie Q., Jain J., Sun M., Kerrich R. and Fan J., 1994. Multiple element analysis of low abundance international reference material BIR-1: results by ICP-MS. Geostandards Newslett., 18: 53-63.

Zhihong W. and Huafu L., 1998. Geology, petrology and geochemistry of the mafic-ultramafic rocks in the Fujian Coastal Region, Southeastern China, and their genesis. Ofioliti, 23: 1-6.

Received, July 30, 2004
Accepted, April 5, 2005